

Effect of Supporting Surface Layers on Catalytic Activities of Gold Nanoparticles in CO Oxidation

Wenfu Yan, Shannon M. Mahurin, Bei Chen, Steven H. Overbury, and Sheng Dai*

Chemical Sciences Division, Oak Ridge National Laboratory, Oak Ridge, Tennessee 37831

Received: April 18, 2005; In Final Form: June 8, 2005

The surfaces of fumed silica materials were modified with a surface sol–gel process for catalysis applications. This surface-modification approach allows not only a monolayer growth of TiO_2 or Al_2O_3 but also a stepwise double-layer growth of $\text{TiO}_2/\text{TiO}_2$, $\text{Al}_2\text{O}_3/\text{Al}_2\text{O}_3$, $\text{TiO}_2/\text{Al}_2\text{O}_3$, or $\text{Al}_2\text{O}_3/\text{TiO}_2$ on the surfaces of the silica materials with a monolayer precision. XRD analyses revealed that the coated monolayers and double layers of TiO_2 and Al_2O_3 were amorphous. Gold nanoparticles were successfully deposited on the above six surface-modified silica materials via a deposition-precipitation method. The catalytic activities of these six gold catalysts for CO oxidation are highly dependent on the structures of their surface monolayers or double layers. The gold catalyst supported on the silica material functionalized with a TiO_2 monolayer (Au/TiO_2) is the most active in both as-synthesized and oxidized forms, while the gold catalyst supported on the silica material functionalized with an $\text{Al}_2\text{O}_3/\text{TiO}_2$ double layer ($\text{Au}/\text{Al}_2\text{O}_3/\text{TiO}_2/\text{SiO}_2$) is the most active in the reduced form among the six catalysts. Surprisingly, the gold catalyst supported on the silica material functionalized with a $\text{TiO}_2/\text{Al}_2\text{O}_3$ double layer ($\text{Au}/\text{TiO}_2/\text{Al}_2\text{O}_3/\text{SiO}_2$) has much less activity than $\text{Au}/\text{Al}_2\text{O}_3/\text{TiO}_2/\text{SiO}_2$ under all various treatments, underscoring the sensitivity of the catalytic activity to the structure of the supporting surfaces.

Introduction

Although gold in bulk has often been regarded to be poorly active as a catalyst, Haruta and co-workers have found that the gold nanoparticles deposited on selected metal oxides exhibited surprisingly high catalytic activity for low-temperature CO oxidation.¹ An extensive literature now exists concerning CO oxidation and selective propylene oxidation catalyzed by gold nanoparticles supported on various metal oxides,^{2,3} such as TiO_2 ,^{4–14} Fe_2O_3 ,^{1,15–17} Co_3O_4 ,¹ NiO ,¹ SiO_2 ,^{18–20} ZrO_2 ,²¹ MgO ,^{22–24} and Al_2O_3 .²⁵ Even though the catalytic mechanism of the gold nanoparticles is not well understood, the nature of the supports is commonly considered to be one of the key factors affecting the catalytic activity and stability of supported gold catalysts. To understand the contribution of oxide supports to the catalytic activity of gold nanoparticles, intensive studies have been initiated in the past several years, primarily using different metal oxide supports. Notably, Grunwaldt et al. prepared two gold model catalysts on the basis of deposition of “size-controlled” gold colloids (~ 2 nm) on TiO_2 and ZrO_2 at a pH lower than the isoelectric points (IEPs) of both metal oxides.⁹ The significant support effect induced by the structural difference between TiO_2 and ZrO_2 was observed, showing that the former is a much more active support than the latter in controlling the catalytic activity of gold catalysts. More recently, Arrii et al. directly deposited metallic Au nanoparticles (~ 3 nm) generated via a laser ablation on high-surface-area metal oxides of $\gamma\text{-Al}_2\text{O}_3$, ZrO_2 , and TiO_2 to determine the influence of the supports on catalytic CO oxidation without the hindrance imposed by the differences in particle size or oxidized gold species.²⁶ By comparing the activities of the different catalysts,

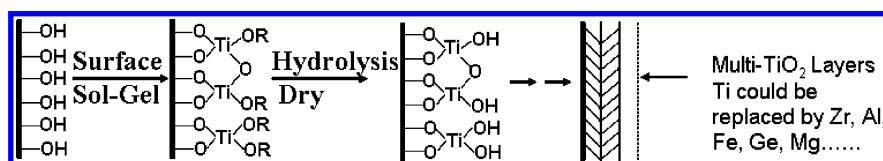
they concluded that the nature of the support directly affects the activity of gold.

Corma and co-workers have recently explored an interesting aspect of the support promotion effects through controlled variation of the particle size of a CeO_2 support.²⁷ The gold nanoparticles deposited on the nanocrystals of cerium oxide via coprecipitation exhibited an increased activity for CO oxidation by 2 orders of magnitude compared with the gold nanoparticles deposited on a regular cerium oxide. This observation has opened up a new dimension in the support studies, indicating that not only the size of gold nanoparticles but also the size of the support oxide has a profound influence on the catalysis properties of gold nanoparticles.

In the present study, we report a new support effect induced by the tailored nanostructure of supporting surface layers on the catalytic activity of CO oxidation by gold nanoparticles. The supporting surface layers were a single surface monolayer of TiO_2 (or Al_2O_3) on silica or surface double layers grown on silica in all four possible combinations of TiO_2 and Al_2O_3 . These supporting surface layers were synthesized on silica surfaces by a surface sol–gel (SSG) process.

The surface sol–gel (SSG) process was originally developed by Kunitake and co-workers.^{28,29} This novel technology enables a molecular-scale control of film thickness over a large 2D substrate area and can be viewed as a solution-based methodology for atomic layer deposition synthesis.³⁰ Compared with conventional deposition methods, the surface sol–gel method has an advantage in producing very thin, conformal films with control of the thickness and composition of the films possible at the atomic level, which is critical for many applications in catalysis for uniformity of supports. The SSG technique generally consists of two half-reactions as shown in Scheme 1: (i) nonaqueous condensation of metal alkoxide precursor molecules with surface hydroxyl groups followed by careful

* Author to whom correspondence should be addressed. E-mail: dais@ornl.gov.

SCHEME 1. The Schematic Diagram for the Basic Coating Protocol for Ultrathin Metal Oxide Layers over a Large 2D Substrate Area**TABLE 1: The Details on the Amount of Chemicals Used in the Growth of One-Layer or Multilayers of Titanium Oxide and Aluminum Oxide on the Surface of Cab-O-Sil SiO₂**

composites	substrate	(g)	precursor (g)		toluene (mL)	methanol (mL)
			Ti(OBu ⁿ) ₄	Al(OBu ⁿ) ₃		
Al ₂ O ₃ /SiO ₂	SiO ₂	9.8	N/A	7.74	70	120
TiO ₂ /SiO ₂	SiO ₂	10.2	7.9	N/A	70	70
Al ₂ O ₃ /TiO ₂ /SiO ₂	TiO ₂ /SiO ₂	2.0	4.9	N/A	20	20
TiO ₂ /Al ₂ O ₃ /SiO ₂	Al ₂ O ₃ /SiO ₂	2.0	N/A	4.8	20	20
Al ₂ O ₃ /Al ₂ O ₃ /SiO ₂	Al ₂ O ₃ /SiO ₂	2.0	N/A	5.0	20	20
TiO ₂ /TiO ₂ /SiO ₂	TiO ₂ /SiO ₂	2.0	5.0	N/A	20	20

nonaqueous washing to remove the unreacted alkoxide precursor and (ii) aqueous hydrolysis of the adsorbed metal alkoxide species to regenerate surface hydroxyls. The iteration of the above sequential condensation and hydrolysis reactions allows the layer-by-layer coating of a selected metal oxide on a hydroxyl-terminated surface. Although the original technique was developed to functionalize 2D oxide surfaces, Huang and Kunitake have recently succeeded in using this technique for fossilization of cellulosic substances.³¹ We have recently extended this methodology to prepare mesoporous materials with tailored pore sizes¹³ and unique SERS substrates with dielectric overlayers.³²

Experimental Section

Synthesis of Monolayers and Double Layers. The silica material used in this investigation is a nonporous fumed silica (Cab-O-Sil, CABOT Co. Tuscola, IL), which has a surface area of 216.5 m² g⁻¹ and a silanol density of 4–8 mmol SiOH/m².³³ The procedure for functionalization of monolayers or double layers of titanium oxide and aluminum oxide on the silica surfaces of Cab-O-Sil was developed according to the method described by Kunitake and co-workers.²⁹ Typically, a preweighed SiO₂ powder sample was loaded into a reflux bottle and dried at 125 °C for 16 h. The bottle was then sealed with a predried rubber septum. Subsequently, the metal oxide precursor and the anhydrous mixture of toluene and methanol were transferred into the bottle through a syringe. The resulting solution was refluxed for 3 h. The final product was filtered, washed several times with anhydrous ethanol, hydrolyzed with deionized water, and dried at 80 °C overnight. The iteration of the above sequential condensation and hydrolysis reactions allows the coating of the second monolayer on the one generated in the previous deposition cycle. The details on the amount of the chemicals used are summarized in Table 1.

Precipitation Deposition of Gold. The deposition–precipitation (DP) procedure used here was based on the method originally developed by Haruta and co-workers.³⁴ First, 3.0 g of hydrogen tetrachloroaurate(III) trihydrate (HAuCl₄·3H₂O, 99.9+%, Aldrich) was dissolved into 500 mL deionized water to form a gold precursor solution. Typically, the pH value of the preweighed gold precursor solution (20 mL) was adjusted to about 10 with vigorous stirring using a solution of 1.0 M KOH at room temperature. The solution was then heated with an 80 °C water bath, and a selected surface-modified SiO₂ (0.4 g) was added with stirring. The resulting cloudy solution was

continually stirred for 2 h. The precipitates were separated by centrifugation and were washed several times with deionized water. The yellow product was dried at 40 °C overnight to get the as-synthesized sample.

Catalysis Test. The CO oxidation reaction was carried out in an AMI 200 (Altamira Instruments). Typically, 50 mg of catalyst was packed into a 4-mm ID quartz U-tube, supported by quartz wool. Sample treatments were carried out on the same instrument using either premixed 8% O₂–He for oxidations or using 50% H₂ mixed with Ar for reductions. During reactions, a gas stream of 1% CO balanced with dry air (<4 ppm water) was flowed at ambient pressure through the catalyst at a rate that was adjusted from sample to sample to maintain a constant space velocity of 44 000 mL/(h·g_{cat}) or about 37 cm³/min. Gas exiting the reactor was analyzed by a Buck Scientific 910 gas chromatograph equipped with dual molecular sieve/porous polymer column (Alltech CTR1) using a thermal conductivity detector. The reaction temperature was varied using an oven or by immersing the U-tube in a dewar of ice water or of cooled acetone by liquid nitrogen, which slowly warmed throughout the approximately 10–20 h taken to measure a light-off curve.

Characterization. Both transmission electron microscopy (TEM) and Z-contrast scanning electron microscopy (STEM) were carried out using a HITACH HD-2000 STEM operated at 200 kV. Powder X-ray diffraction (XRD) data were collected via a Siemens D5005 diffractometer with Cu Kα radiation (λ = 1.5418 Å). Inductively coupled plasma (ICP) analysis was performed on IRIS Intrepid II XSP spectrometer (Thermo Electron Corporation), and each measurement was repeated three times. Nitrogen gas adsorption measurements (Micromeritics Gemini) were used to determine the surface areas of surface-modified Cab-O-Sil samples.

Results and Discussions

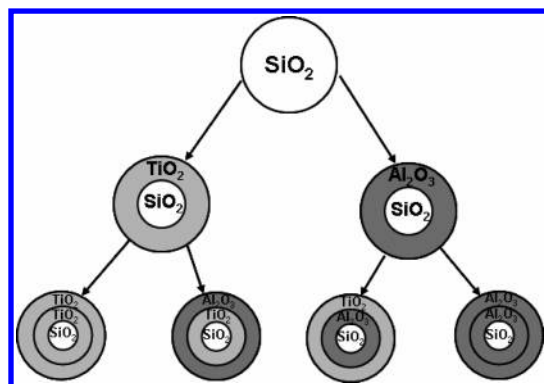
The main surfaces discussed here consist of two sequential combinations of TiO₂ and Al₂O₃ monolayers on amorphous silica: (1) Al₂O₃/TiO₂/SiO₂ (SiO₂ coated with a first layer of TiO₂ and then with a second layer of Al₂O₃) and (2) TiO₂/Al₂O₃/SiO₂ (SiO₂ coated with a first layer of Al₂O₃ and then a second layer of TiO₂). For comparison, we have also prepared the same silica sample functionalized by TiO₂ (TiO₂/SiO₂) or Al₂O₃ (Al₂O₃/SiO₂) monolayer or by two sequential layers (double layer) of TiO₂ (TiO₂/TiO₂/SiO₂) or Al₂O₃ (Al₂O₃/Al₂O₃/SiO₂). The schematic diagram for the various combinations of ultrathin TiO₂ and Al₂O₃ layers on fumed SiO₂ are shown in Scheme 2.

TABLE 2: The Experimental ICP Results (Metal Loading) for Au/Al₂O₃/SiO₂, Au/TiO₂/SiO₂, Au/Al₂O₃/Al₂O₃/SiO₂, Au/TiO₂/TiO₂/SiO₂, Au/Al₂O₃/TiO₂/SiO₂, and Au/TiO₂/Al₂O₃/SiO₂^a

catalyst	Au wt%	Al wt%	Ti wt%	first:second layer (mol)	coverage (first layer)
Au/Al ₂ O ₃ /SiO ₂	7.9	4.6	N/A	N/A	160%
Au/Al ₂ O ₃ /Al ₂ O ₃ /SiO ₂	10.3	14.2	N/A	1:2.1	N/A
Au/TiO ₂ /Al ₂ O ₃ /SiO ₂	11.7	3.5	16.3	1:2.6	N/A
Au/TiO ₂ /SiO ₂	5.1	N/A	0.8	N/A	13.5%
Au/TiO ₂ /TiO ₂ /SiO ₂	6.8	N/A	3.1	1:3.0	N/A
Au/Al ₂ O ₃ /TiO ₂ /SiO ₂	10.3	17.7	0.7	1:47.6	N/A

^a The BET surface area of Cab-O-Sil is 216.5 m²/g. The average surface Si—OH density is 6 μmol/m².

SCHEME 2. The Schematic Diagram for the Basic Coating Protocol for Ultrathin TiO₂ and Al₂O₃ Layers on Fumed SiO₂



The elemental compositions of the supporting surfaces were determined through ICP analyses of the digestion solutions obtained via dissolution of the surface-modified silica samples in HF/HCl/HNO₃. Table 2 shows the measured weight percents (wt %) of Au, Ti, and Al obtained from ICP results for the six surface-modified SiO₂ supports. It is of interest to determine the equivalent number of the surface monolayers obtained for each deposition to provide an indication of the extent to which the layer-by-layer deposition is achieved by the SSG process. For both single- and double-layer depositions, the Ti and Al species are assumed to be present as —Ti(OH)₃ and —Al(OH)₃, respectively. On the basis of this approximation, the first-layer coverages were computed in units of the surface silanol density (6 μmole/m²)³³ and are given in Table 2 along with the ratio of the second layer to the first layer.

The measured titanium content of the TiO₂/SiO₂ support is 0.8 wt %, giving rise to a 13% coverage. The low surface coverage of titanium species indicates that most of the surface silanols are not functionalized by titanium species via formation of Si—O—Ti linkages. Either a high fraction of silanols are unavailable for functionalization or the functionalization is kinetically limited. In contrast, the aluminum content of the Al₂O₃/SiO₂ support is equivalent to a 160% coverage. This overcoverage of SiO₂ surfaces by Al₂O₃ via the SSG process can be attributed to two factors. First, the reactivity of aluminum alkoxide with SiOH groups may be higher than that of titanium alkoxide, which allows most of the SiOH sites to react with aluminum alkoxide to form Si—O—Al linkages. Second, dimeric and oligomeric aluminum species were attached to a single SiOH site. The existence of dimeric and tetrameric aluminum alkoxides has been well documented in the literature. For example, both spectroscopical investigations³⁵ and single-crystal X-ray structure determinations³⁶ have shown the tetrameric character of aluminum isopropoxide in both solution and solid states. The dimeric species of [Al(OBu)₃]₂ has also been reported.³⁷ Therefore, a single SiOH site can attach two or more aluminum species, leading to the overcoverage of silica surfaces.

The total titanium content of the double-layer sample TiO₂/TiO₂/SiO₂ is 3.1 wt %. Accordingly, the mole ratio of the second-layer titanium content to the first-layer titanium content is close to 3.0:1.0 on the basis of the ICP analyses. This result can be explained as follows. The low coverage of the first-layer functionalization indicates that most of the TiO₂ precursor species are attached to Si—OH groups in the form of —Si—O—Ti(OPr)₃ and are highly dispersed on silica surfaces without cross-linking. Each functionalized surface site [—Si—O—Ti(OPr)₃] can generate three titanol sites during subsequent hydrolysis, available for the second-layer functionalization, which is in perfect agreement with the observed 3:1 ratio. In this model, the growth of the second layer can be viewed as a dendritic growth process occurring primarily on the titania layers and is consistent with the layer-by-layer characteristics of the SSG process.²⁹ However, we cannot eliminate the possibility that additional growth occurs on the unfunctionalized silanols during the second-layer depositions.

In the case of the double-layer sample Al₂O₃/Al₂O₃/SiO₂, the mole ratio of the second-layer aluminum content to the first-layer aluminum content is 2.1:1.0, suggesting that some of the aluminum alkoxide sites generated by the first-layer functionalization are cross-linked during the hydrolysis step. Therefore, a limited dendritic growth is expected so that the mole ratio of the second-layer aluminum content to the first-layer aluminum content deviates from 3:1. In the case of Al₂O₃/TiO₂/SiO₂, the mole ratio of Al to Ti is as high as 47.6:1 on the basis of ICP analysis. This high mole ratio indicates that the aluminum alkoxide not only undergoes the oligomeric attachment but also reacts with the titanols and the unreacted silanols leftover from the first-layer functionalization. Hence, the reactivity of Al(OBu)₃ with silica surfaces is higher than that of Ti(OBu)₃ with silica surfaces, which has been observed previously by Kunitake and co-workers for planar silica surfaces. In the reverse case in which titania is deposited onto alumina layer (TiO₂/Al₂O₃/SiO₂), the titania reacts very readily, giving rise to high Ti loading. The second-to-first layer ratio of 2.6:1 suggests that the titania functionalizes a high fraction of the alumina hydroxyl surface species.

The elemental analyses of samples Au/Al₂O₃/SiO₂, Au/TiO₂/SiO₂, Au/Al₂O₃/Al₂O₃/SiO₂, Au/TiO₂/TiO₂/SiO₂, Au/Al₂O₃/TiO₂/SiO₂, and Au/TiO₂/Al₂O₃/SiO₂ for gold contents showed that the gold-weight loadings of these six samples were 7.9, 5.1, 10.3, 6.8, 10.3, and 11.7%, respectively. The above differences in the gold loadings introduced via DP can be qualitatively attributed to the surface-charging properties of these six samples. For example, the isoelectric points (IEPs) of SiO₂, TiO₂, and Al₂O₃ are 2.2, 6.6, and 9.1, respectively. Accordingly, the surface modified with Al₂O₃ is more positively charged than the unmodified silica or the surface modified with TiO₂ under similar aqueous conditions (pH 10). Therefore, the alumina-modified surface should interact more favorably with negatively charged gold precursors during the DP process. This explains why the gold loading of Au/Al₂O₃/SiO₂ is greater than that of

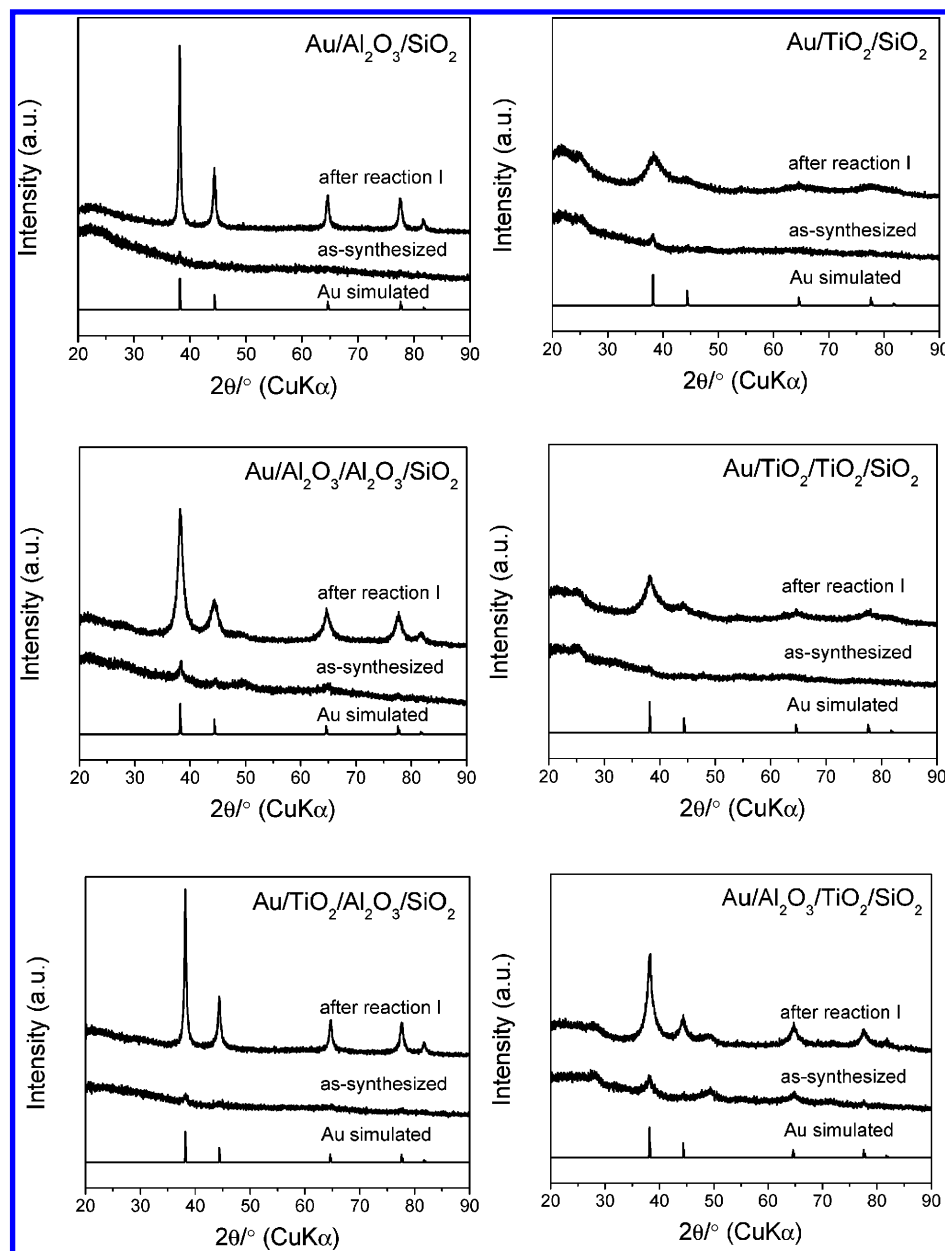


Figure 1. The simulated XRD pattern of Au and experimental XRD patterns for both as-synthesized and after running the light-off curve of the as-synthesized catalysts without pretreatment (reaction I).

Au/TiO₂/SiO₂ and why the gold loadings on the titania only surfaces are lower than those of the alumina-terminated surfaces. Similarly, because the gold precursor species interacts weakly or even repulsively with the silica surface, the low Ti loading is also a factor in causing low Au loadings for the samples functionalized with a titania single layer or double layer. In this case, it is expected that the titania moieties provide the platform for Au hydroxide nucleation. Finally, the Au/TiO₂/Al₂O₃/SiO₂ sample has a high loading because in this case, a high, probably uniform Ti loading is achieved during the second-layer functionalization. The XRD analyses shown in Figure 1 revealed that both monolayers and double layers on the surfaces of the fumed silica were amorphous. For the as-synthesized catalysts, only a very weak Au(111) peak was observed in the XRD patterns, which indicated that most of the Au species in the as-synthesized catalysts are in a cationic oxidation state (hydroxide) and are highly dispersed. The high dispersion of the cationic gold precursors for the as-synthesized catalysts was also confirmed by a high-angle, annular dark field STEM (Z-contrast TEM) investigation. For example, Figure 2 a shows a

dark-field TEM image of the as-synthesized Au/Al₂O₃/Al₂O₃/SiO₂. In Z-contrast TEM, heavy atoms (such as gold) stand out very clearly on a light background of silicon, aluminum, titanium, and oxygen. The tiny, highly uniform bright spots (0.8–4.0 nm diameter) in Figure 2a correspond to the deposited gold precursor species.

For all catalysts, cationic gold species were reduced by the reactant mixture during the catalytic measurements, as indicated by the color change from yellow to black. The XRD analyses of the samples after catalytic measurements (Figure 1) indicate the appearance of very sharp XRD peaks corresponding to reduced Au for the catalysts containing the aluminum-oxide overlayers. However, only very broad Au XRD peaks are observed for the catalysts containing only titanium-oxide overlayers. These observations reveal that the gold nanoparticles on Al₂O₃ surfaces are more susceptible to aggregation than those on TiO₂ surfaces even under ambient conditions. The Z-contrast TEM investigation shown in Figure 2b also revealed that there was a significant aggregation during the reduction of the as-synthesized Au/Al₂O₃/Al₂O₃/SiO₂. However, considerable num-

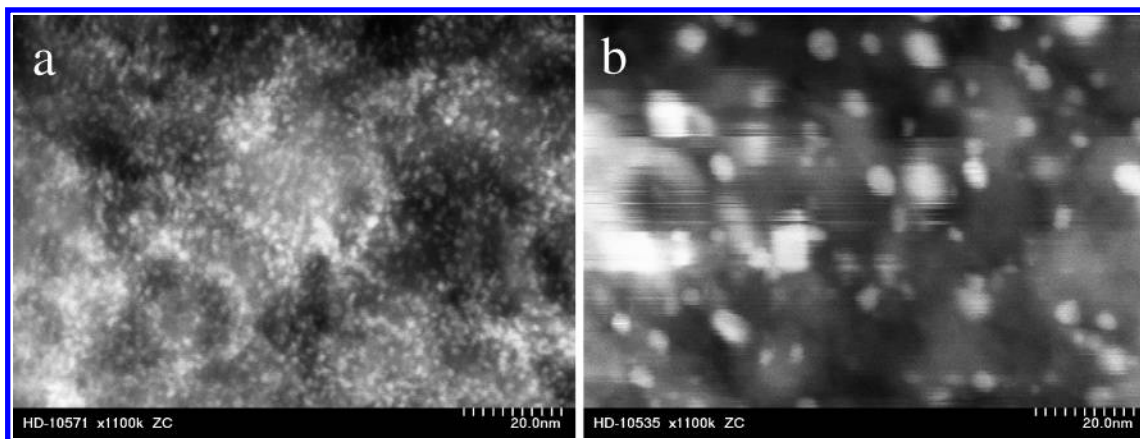


Figure 2. The Z-contrast TEM images of the as-synthesized (a) and reduced (b) Au/Al₂O₃/Al₂O₃/SiO₂ catalysts.

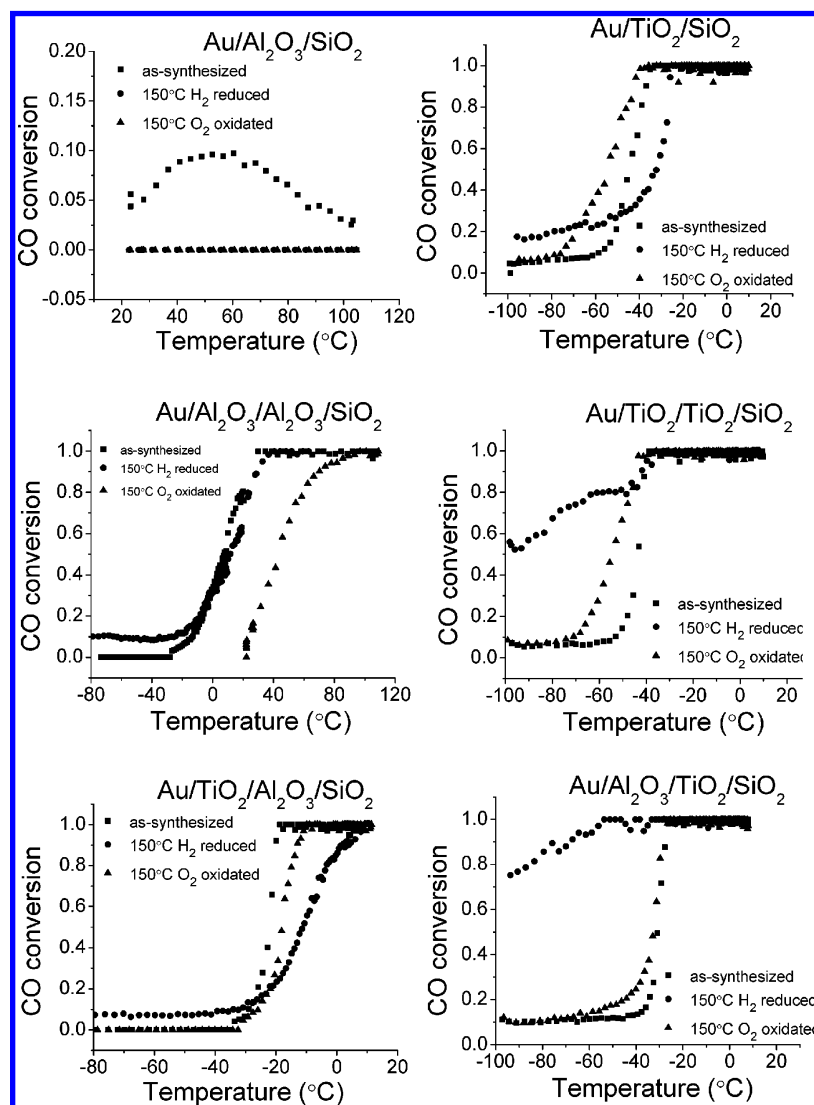


Figure 3. The light-off curves of Au/Al₂O₃/SiO₂, Au/TiO₂/SiO₂, Au/Al₂O₃/Al₂O₃/SiO₂, Au/TiO₂/TiO₂/SiO₂, Au/Al₂O₃/TiO₂/SiO₂, and Au/TiO₂/Al₂O₃/SiO₂. These light-off curves were measured from the samples of both as-synthesized and pretreated under the following conditions: 150 °C in H₂ (50% H₂/He) and 150 °C in O₂ (8% O₂/He).

bers of gold nanoparticles with size <3 nm still exist in the reduced sample.

Figure 3 shows the catalytic light-off curves for Au catalysts derived from the six layered supports tested for CO oxidation. These light-off curves were measured for both as-synthesized and posttreated samples. Two posttreatment conditions were used: 150 °C in H₂ (50% H₂/He) and 150 °C in O₂ (8%

O₂/He). Activities can be qualitatively assessed by the temperatures (T_{50}) at which a 50% conversion of CO to CO₂ is achieved. The values for T_{50} are collected in Table 3.

As a comparison, a sample of unmodified fumed silica was prepared by the identical DP method. This sample shows no measurable CO conversion even at temperatures as high as 160 °C (not shown). This observation is consistent with the results

TABLE 3: Activity (T_{50} °C) for Catalysts after Various Pretreatments

catalyst	Au loading wt%	as-syn.	150 °C in H_2	150 °C in O_2
Au/Al ₂ O ₃ /SiO ₂	7.9	unstable	N/A	N/A
Au/Al ₂ O ₃ /Al ₂ O ₃ /SiO ₂	10.3	7.8	12	43
Au/TiO ₂ /Al ₂ O ₃ /SiO ₂	11.7	-22	-11	-18
Au/TiO ₂ /SiO ₂	5.1	-44	-32	-54
Au/TiO ₂ /TiO ₂ /SiO ₂	6.8	-45	-95	-55
Au/Al ₂ O ₃ /TiO ₂ /SiO ₂	10.3	-31	<-98	-32

previously reported.¹³ Because the IEP of SiO₂ is only ~ 2.2 , the interaction of SiO₂ with gold precursor species is very weak during DP (pH = 6–10), resulting in very small gold loading but large gold particles. Furthermore, the color of the sample obtained via DP of the gold species on the fumed silica is purple, which indicates that the gold species on the SiO₂ surface are reduced.³⁸ The TEM imaging of the gold-deposited sample reveals that the size of the gold nanoparticles is too big (>8 nm) to be catalytically active.¹³

No clear improvement of the catalytic activities was observed for the gold nanoparticles on the fumed silica whose surface was modified with an Al₂O₃ monolayer through the SSG process. The as-synthesized Au/Al₂O₃/SiO₂ sample had a very low conversion at high temperature but was quickly deactivated. The initial apparent conversion can be attributed to stoichiometric CO consumption by the reduction of the gold cationic species, which disappeared after the gold cationic species were totally reduced. This conjuncture is also consistent with the observations that the catalysts pretreated at 150 °C both in H_2 and in O_2 exhibit no activities. Sharp Au lines in the XRD measurements in Figure 1 prove that large Au particles are formed under the reaction conditions, and this large particle size is the probable explanation of the poor activity. Compared with the fumed silica modified with a single Al₂O₃ monolayer, the substrate modified with an Al₂O₃ double layer had a higher gold loading, 10.3 wt % versus 7.9 wt %, and it exhibited moderate, stable activity for CO oxidation. The as-synthesized catalyst reached 50% conversion at 7.8 °C, but T_{50} was increased by the treatments at 150 °C in either H_2 or O_2 . The higher activity obtained for the double-layer catalysts compared to the single layer cannot be explained by the 30% increase in Au loading. Therefore, the second layer of Al₂O₃ must exhibit some additional effect upon the catalytic activity.

Compared to the Al₂O₃-modified fumed silica, the single-layer TiO₂-modified fumed silica (TiO₂/SiO₂) is a better substrate for the preparation of highly active gold nanocatalysts.

For the as-synthesized catalyst, the T_{50} value is -44 °C. Treatment at 150 °C in H_2 decreased the activity slightly (T_{50} = -32 °C), while the treatment at the same temperature in O_2 increased the activity of this catalyst (T_{50} = -54 °C). A single, fractional (0.13) monolayer of titania, grafted to the silica, can completely alter the behavior of the resulting Au catalysts compared to the unmodified silica support. Its activity is higher than the Au catalysts derived from either Al₂O₃-modified silica despite lower Au loadings. The further surface modification of the TiO₂-modified fumed silica by a second TiO₂ monolayer has little further effect upon the activity. The as-synthesized samples of single-layer and double-layer derived catalysts have virtually the same T_{50} values, as they do after treatment at 150 °C in O_2 . Clearly, the catalytic activity depends weakly on the number of the monolayers under these reaction and treatment conditions. Treating in H_2 at 150 °C dramatically altered the light-off curve of catalyst Au/TiO₂/TiO₂/SiO₂, giving rise to an anomalously slow-temperature variation in the conversion below -50 °C. This observation is consistent with those reported previously.³⁹ Haruta attributed this anomalous catalytic activity to the formation of carbonate species condensed on the catalyst surfaces at low temperature.³⁹

The deposition of gold nanoparticles on the mixed double-layer-coated supports (Au/TiO₂/Al₂O₃/SiO₂ and Au/Al₂O₃/TiO₂/SiO₂) also gave rise to two active catalysts for CO oxidation. Of the two mixed layer supported catalysts in either the as-synthesized state or after treatment at 150 °C in O_2 , the sample with the outer alumina termination (Au/Al₂O₃/TiO₂/SiO₂) provides slightly lower T_{50} and therefore higher activity. Similarly as for the catalyst functionalized with a TiO₂ double layer, treating in H_2 at 150 °C dramatically altered the light-off curve of catalyst Au/Al₂O₃/TiO₂/SiO₂, giving rise to an anomalously slow-temperature variation in the conversion below -50 °C but apparently very high activity.

The differences between Au/TiO₂/Al₂O₃/SiO₂ and Au/Al₂O₃/TiO₂/SiO₂ in the catalytic activities indicate the sensitivity of gold catalysts to the local surface structures. Figure 4 shows the high-magnification Z-contrast TEM images of Au/Al₂O₃/TiO₂/SiO₂ (a) and Au/TiO₂/Al₂O₃/SiO₂ (b) after the treatments at 150 °C in H_2 . The Z-contrast images recorded at identical magnification show a clear difference in size distribution (see Supporting Materials, Figure s1, the particle size distribution calculated from TEM images). More small gold nanoparticles (<2 nm) were found on the surface of the reduced Au/Al₂O₃/TiO₂/SiO₂, while the population of small gold nanoparticles was considerably less on the surface of the reduced Au/TiO₂/Al₂O₃/

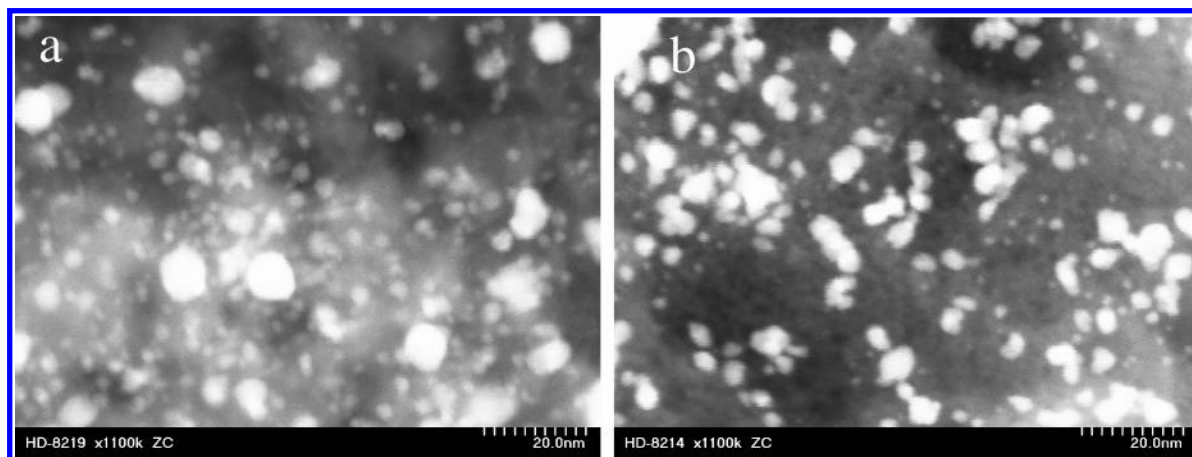


Figure 4. The Z-contrast transmission electron microscopy (TEM) images of the reduced Au/Al₂O₃/TiO₂/SiO₂ (a) and Au/TiO₂/Al₂O₃/SiO₂ (b) at 150 °C in H_2 .

TABLE 4: Au Particle Diameters in Reduced Samples Calculated from Au(111) Peak

catalyst	Au/Al ₂ O ₃ /SiO ₂	Au/Al ₂ O ₃ /Al ₂ O ₃ /SiO ₂	Au/TiO ₂ /Al ₂ O ₃ /SiO ₂
diameter (nm)	24.5	8.0	21.3
catalyst	Au/TiO ₂ /SiO ₂	Au/TiO ₂ /TiO ₂ /SiO ₂	Au/Al ₂ O ₃ /TiO ₂ /SiO ₂
diameter (nm)	2.7	3.8	7.7

SiO₂. This observation was consistent with the analysis results of the corresponding XRD patterns of metallic gold in Figure 1 (see the discussions in the next paragraph). Accordingly, a stronger interaction of gold nanoparticles with the Al₂O₃/TiO₂/SiO₂ surface than that with the TiO₂/Al₂O₃/SiO₂ surface is indicated, evidently because of a higher barrier for particle coarsening on the former surface. This conclusion is supported by addition treatments performed at 300 and 500 °C. The activity remains higher for the Au/Al₂O₃/TiO₂/SiO₂ sample following these treatments. (see Figure S2, Supporting Materials).

To correlate metallic gold particle sizes to catalytic activities, the diffraction peak of Au(111) in each reduced XRD pattern shown in Figure 1 was fitted to a Lorentzian distribution using a Levenberg–Marquardt χ^2 minimization procedure to obtain an estimation of average particle sizes on the basis of the corresponding full width at half-maximum (fwhm). The gold-particle diameters were subsequently calculated from the fwhm's of the XRD peaks using Sherrer's equation:⁴⁰

$$D = \frac{k\lambda}{\beta \cos \theta}$$

where k is a constant (0.94), λ is the wavelength of the radiation (Cu K α = 1.5418 Å), β is the fwhm of the peak in radians, and θ is the Bragg angle. The analyses results are summarized in Table 4. As seen from Table 4, the average Au particle size of the reduced Au/TiO₂/SiO₂ sample is the smallest among the six catalysts. The high catalytic activity of this sample (Table 3) indicates that the high dispersion and stabilization of small gold particles is a key factor in determining catalytic activities of gold catalysts. The Au particle size of the reduced Au/Al₂O₃/TiO₂/SiO₂ sample is about 3 times smaller than that of the reduced Au/TiO₂/Al₂O₃/SiO₂ sample, which seems to be inconsistent with the particle-size distribution obtained from the high magnification Z-contrast TEM images (Figure 4). To investigate this inconsistency, the Z-contrast TEM imaging of both samples with a lower magnification was conducted to survey larger sample areas. At the lower magnification, many particles distributed in the range of 10–40 nm are visible on reduced Au/TiO₂/Al₂O₃/SiO₂, which are not observed on reduced Au/Al₂O₃/TiO₂/SiO₂ (see Supporting Information, Figure S3). This observation is qualitatively consistent with the result from the XRD analysis and is in a qualitative agreement with the results of the catalysis activities showing that the latter catalyst is more active than the former. The average Au-particle size of the reduced Au/Al₂O₃/Al₂O₃/SiO₂ sample is comparable with that of the reduced Au/Al₂O₃/TiO₂/SiO₂ sample but is about 3 times smaller than that of the reduced Au/TiO₂/Al₂O₃/SiO₂ sample. Surprisingly, the catalytic activity of the reduced Au/Al₂O₃/Al₂O₃/SiO₂ sample is much worse than those of the reduced Au/TiO₂/Al₂O₃/SiO₂ sample and the reduced Au/Al₂O₃/TiO₂/SiO₂ sample. This observation indicates that the Au particle size is not the only factor in determining the catalytic activity of gold catalysts. The support compositions also have a profound influence.

In conclusion, a surface-modification methodology based on the surface sol–gel synthesis has been developed to tailor the surfaces of amorphous silica materials for catalysis applications. The essence of this methodology is to generate the amorphous oxide layers with controlled composition and conformity on silica surfaces. Both surface compositions and postsynthesis treatments of the catalyst supports have been demonstrated to play important roles in determining the activities and stabilities of the gold nanocatalysts. The activity of Au/Al₂O₃/TiO₂/SiO₂ is higher than that of Au/TiO₂/Al₂O₃/SiO₂ for CO oxidation. This observation indicates that the surface-functionalization sequence is an important factor in determining the catalytic activities of the gold nanoparticles deposited on the surface-modified fumed silica supports.

Acknowledgment. This work was conducted at the Oak Ridge National Laboratory and was supported by the Division of Chemical Sciences, Office of Basic Energy Sciences, U.S. Department of Energy, under contract No. DE-AC05-00OR22725 with UT-Battelle, LLC. This research was supported in part by an appointment for W.Y. to the Oak Ridge National Laboratory Postdoctoral Research Associates Program administered jointly by the Oak Ridge Institute for Science and Education and Oak Ridge National Laboratory.

Supporting Information Available: Au particle size distribution in both reduced Au/Al₂O₃/TiO₂/SiO₂ and Au/TiO₂/Al₂O₃/SiO₂ calculated from their TEM images, Figure S1. The light-off curves of Au/Al₂O₃/TiO₂/SiO₂ and Au/TiO₂/Al₂O₃/SiO₂ treated at 300 °C and 500 °C in O₂, Figure S2. This material is available free of charge via the Internet at <http://pubs.acs.org>.

References and Notes

- (1) Haruta, M.; Yamada, N.; Kobayashi, T.; Iijima, S. *J. Catal.* **1989**, *115*, 301.
- (2) Bond, G. C.; Thompson, D. T. *Catal. Rev.—Sci. Eng.* **1999**, *41*, 319.
- (3) Hutchings, G. J. *Gold Bull.* **2004**, *37*, 3.
- (4) Moreau, F.; Bond, G. C.; Taylor, A. O. *Chem. Commun.* **2004**, 1642.
- (5) Valden, M.; Lai, X.; Goodman, D. W. *Science* **1998**, *281*, 1647.
- (6) Chen, M. S.; Goodman, D. W. *Science* **2004**, *306*, 252.
- (7) Stangland, E. E.; Stavens, K. B.; Andres, R. P.; Delgass, W. N. *J. Catal.* **2000**, *191*, 332.
- (8) Lin, S. D.; Bollinger, M.; Vannice, M. A. *Catal. Lett.* **1993**, *17*, 245.
- (9) Grunwaldt, J. D.; Kiener, C.; Wogerbauer, C.; Baiker, A. *J. Catal.* **1999**, *181*, 223.
- (10) Grunwaldt, J. D.; Baiker, A. *J. Phys. Chem. B* **1999**, *103*, 1002.
- (11) Dekkers, M. A. P.; Lippits, M. J.; Nieuwenhuys, B. E. *Catal. Lett.* **1998**, *56*, 195.
- (12) Yan, W. F.; Chen, B.; Mahurin, S. M.; Dai, S.; Overbury, S. H. *Chem. Commun.* **2004**, 1918.
- (13) (a) Yan, W. F.; Chen, B.; Mahurin, S. M.; Hagaman, E. W.; Dai, S.; Overbury, S. H. *J. Phys. Chem. B* **2004**, *108*, 2793. (b) Yan, W. F.; Petkov, V.; Mahurin, S. M.; Overbury, S. H.; Dai, S. *Catal. Commun.* **2005**, *6*, 404.
- (14) Yan, W. F.; Chen, B.; Mahurin, S. M.; Schwartz, V.; Mullins, D. R.; Lupini, A. R.; Pennycook, J.; Dai, S.; Overbury, S. H. *J. Phys. Chem. B* **2005**, *109*, 10676.
- (15) Kahlich, M. J.; Gasteiger, H. A.; Behm, R. J. *J. Catal.* **1999**, *182*, 430.
- (16) Schubert, M. M.; Hackenberg, S.; van Veen, A. C.; Muhler, M.; Plzak, V.; Behm, R. J. *J. Catal.* **2001**, *197*, 113.
- (17) Boccuzzi, F.; Chiorino, A.; Manzoli, M.; Andreeva, D.; Tabakova, T. *J. Catal.* **1999**, *188*, 176.
- (18) Liu, J. H.; Wang, A. Q.; Chi, Y. S.; Lin, H. P.; Mou, C. Y. *J. Phys. Chem. B* **2005**, *109*, 40.
- (19) Date, M.; Okumura, M.; Tsubota, S.; Haruta, M. *Angew. Chem., Int. Ed.* **2004**, *43*, 2129.
- (20) Overbury, S. H.; Ortiz-Soto, L.; Zhu, H. G.; Lee, B.; Amiridis, M. D.; Dai, S. *Catal. Lett.* **2004**, *95*, 99.

- (21) Knell, A.; Barnickel, P.; Baiker, A.; Wokaun, A. *J. Catal.* **1992**, 137, 306.
- (22) Yoon, B.; Hakkinen, H.; Landman, U.; Worz, A. S.; Antonietti, J. M.; Abbet, S.; Judai, K.; Heiz, U. *Science* **2005**, 307, 403.
- (23) Guzman, J.; Gates, B. C. *J. Am. Chem. Soc.* **2004**, 126, 2672.
- (24) Molina, L. M.; Hammer, B. *Phys. Rev. Lett.* **2003**, 90, 206102.
- (25) Bethke, G. K.; Kung, H. H. *Appl. Catal., A* **2000**, 194, 43.
- (26) Arri, S.; Morfin, F.; Renouprez, A. J.; Rousset, J. L. *J. Am. Chem. Soc.* **2004**, 126, 1199.
- (27) Carrettin, S.; Concepcion, P.; Corma, A.; Nieto, J. M. L.; Puentes, V. F. *Angew. Chem., Int. Ed.* **2004**, 43, 2538.
- (28) Ichinose, I.; Senzu, H.; Kunitake, T. *Chem. Lett.* **1996**, 831.
- (29) Ichinose, I.; Senzu, H.; Kunitake, T. *Chem. Mater.* **1997**, 9, 1296.
- (30) Leskela, M.; Ritala, M. *Angew. Chem., Int. Ed.* **2003**, 42, 5548.
- (31) Huang, J.; Kunitake, T. *J. Am. Chem. Soc.* **2003**, 125, 11834.
- (32) Bao, L. L.; Mahurin, S. M.; Dai, S. *Anal. Chem.* **2004**, 76, 4531.
- (33) Nawrocki, J. *J. Chromatogr., A* **1997**, 779, 29.
- (34) Tsubota, S.; Haruta, M.; Kobayashi, T.; Ueda, A.; Nakahara, Y. *Stud. Surf. Sci. Catal.* **1991**, 63, 695.
- (35) Mehrotra, R. C.; Rothwell, I.; Singh, A.; Bradley, D. C. *Alkoxo and Aryloxo Derivatives of Metals*; Academic Press: San Diego, CA, 2002.
- (36) Foltz, K.; Streib, W. E.; Caulton, K. G.; Poncelet, O.; Hubert-pfalzgraf, L. G. *Polyhedron* **1991**, 10, 1639.
- (37) Cayton, R. H.; Chisholm, M. H.; Davidson, E. R.; Distasi, V. F.; Du, P.; Huffman, J. C. *Inorg. Chem.* **1991**, 30, 1020.
- (38) Mukherjee, P.; Patra, C. R.; Ghosh, A.; Kumar, R.; Sastry, M. *Chem. Mater.* **2002**, 14, 1678.
- (39) Haruta, M. *Cattech* **2002**, 6, 102.
- (40) Suryanarayana, C.; Norton, M. G. *X-ray diffraction*; Plenum Press: New York, 1998.